JOURNAL OF GEOPHYSICAL RESEARCH, VOL. 102, NO. C1, PAGES 1101–1117, JANUARY 15, 1997

Winter snow cover on sea ice in the Weddell Sea

Robert A. Massom
Antarctic Cooperative Research Centre, University of Tasmania, Hobart, Tasmania, Australia

Mark R. Drinkwater
NASA Jet Propulsion Laboratory, California Institute of Technology, Pasadena

Christian Haas
Alfred Wegener Institut für Polar- und Meeresforschung, Bremerhaven, Germany

Abstract. Measurements of snow thickness, temperature, salinity, density, and stratigraphy acquired during the 1992 Winter Weddell Gyre Study are presented. Results indicate that the winter snow cover on sea ice in the Weddell Sea is extremely variable. Extreme fluctuations in Antarctic synoptic conditions (air temperature, precipitation, humidity, and wind speed) occur during the austral winter. They result in unique modifications and additions to the snow layer during the aging process and act to stabilize an otherwise easily wind-redistributed shallow snow cover and develop well-packed drift features. The latter occur even over relatively undeformed areas of sea ice and have a significant localized effect on the snow thickness distribution. Significant variability in snow grain size (mean 2.73 ± 3.12 mm) and density (0.32 ± 0.09 g cm^{-3}) is observed as a result of cyclical switches between high- and low-temperature gradient metamorphism. Multiple icy layers indicate multiple thaw-freeze events. One such event occurred during a 3-day station, during which the air temperature rose by 22°C in 12 hours (to approximately 0°C). This paper also examines mechanisms for flooding of the snow-ice interface, including snow loading. Even where the latter is not a factor, the layer of snow immediately above the snow-ice interface is commonly damp and saline (>10‰). Limitations in the data set are discussed, and comparisons are drawn with other experiments.

1. Introduction

Antarctic sea ice intercepts solid precipitation that would otherwise fall into the ocean. By forming a dynamic insulative lid between ocean and atmosphere and by virtue of its great seasonal variability in areal extent (from ~4–20 × 10^6 km^2 [*Gloersen et al.*, 1992]), this combined layer of snow and ice plays a significant role in modifying high-latitude and global biogeophysical processes. As it accumulates and redistributes, the snow exhibits unique optical and thermal properties and variability on a variety of timescales and space scales [*Worby and Massom*, 1995]. On long temporal scales, model results indicate that the accumulation of snow, with its relatively high albedo, on sea ice has a net cooling effect on global climate [*Ledley*, 1991], although shortwave fluxes are low during most of the growth season [*Eicken et al.*, 1995]. By virtue of its low thermal conductivity, snow affects the energy and mass balance of sea ice on both seasonal and synoptic scales [*Eicken et al.*, 1995; *Maykut*, 1986; *Owens and Lemke*, 1990]. It also makes a direct and significant contribution to the overall mass balance of the Antarctic pack by the refreezing of slush, termed snow-ice formation in recent papers [*Eicken et al.*, 1994; *Lytle and Ackley*, 1992]. Simulations by *Eicken et al.* [1995] demonstrate that the presence of a snow cover increases ice brine volume by a factor of 1.5–2, thereby affecting ice strength. Snow accumulation modifies ice surface roughness and consequently the ice-air drag coefficient [*Andreas et al.*, 1993; *Banke et al.*, 1980] and the bulk transfer coefficients for latent and sensible heat [*Andreas*, 1987]. A winter snow cover thus modifies the rate at which the underlying sea ice loses heat to the atmosphere, reducing the capacity for thermodynamic ice growth and brine rejection into the ocean. Also, a spring/summer snow layer acts as a protective buffer, retarding sea ice surface melt.

The time-space history of snow, from deposition both into leads and onto ice and through its redistribution by ice drift and snow drift until its subsequent melting, therefore regulates the freshwater flux and salinity budget of the upper ocean. These processes in turn affect water mass formation and modification [*Gordon and Huber*, 1990]. Biologically, varying snow cover characteristics regulate the intensity and spectral composition of incoming shortwave radiation available to sea ice microalgae for photosynthesis [*Eicken*, 1992; *Sullivan et al.*, 1985].

Large-scale satellite remote-sensing studies in both polar regions [e.g., *Comiso*, 1983; *Drinkwater*, 1989; *Garrity*, 1992; *Livingstone et al.*, 1987; *Mätzler et al.*, 1984a, b] suggest that snow cover variability can have a first-order effect on the observed surface microwave signature. By studying shipborne radar data and calibrated backscatter results from the ERS 1 synthetic aperture radar (SAR) collected during the experiment described in this paper, *Drinkwater and Haas* [1994] and *Drinkwater et al.* [1995] show that a thin, dry snow cover is largely transparent to centimeter wavelengths and the surface contribution to radar backscatter intensity is negligible (at the ~23° incidence angle of the ERS 1 and 2 SARs), with the

Paper number 96JC02992.
0148-0227/97/96JC-02992$09.00

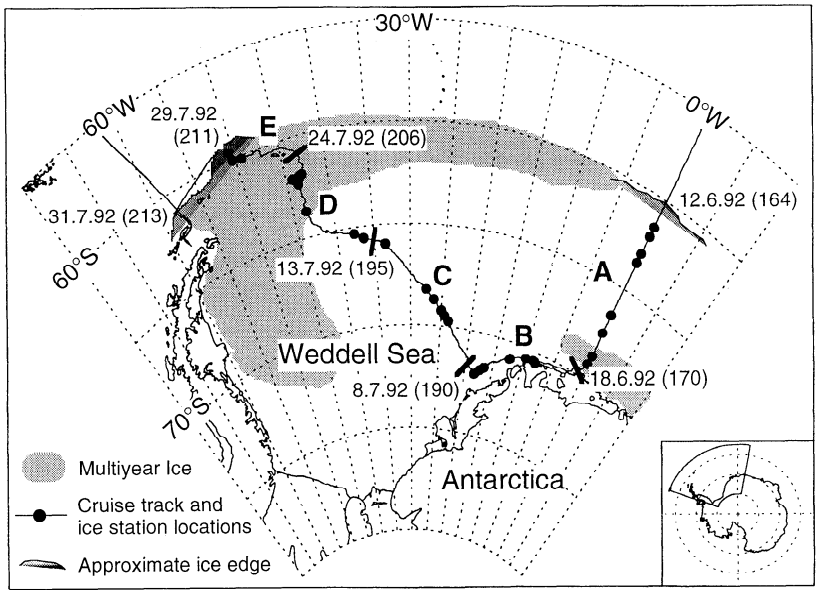

Figure 1. The cruise track of RV *Polarstern* during the Winter Weddell Gyre Study, May–August 1992, showing sectors with common ice conditions, labeled A–E. Multiyear ice extent is an approximation derived from enhanced-resolution ERS 1 scatterometer data by *Drinkwater et al.* [1993b].

primary scattering originating from the snow-ice interface. This is not the case, however, for a wet or saline snow cover. Liquid water content or salinity drastically increases the absorption and power reflection coefficient (R), and the contribution of snow surface roughness to the measured backscatter is significant [*Drinkwater et al.*, 1993a]. The presence of a slush layer can modify the small-scale surface roughness of the floe and can create an artificial dielectric surface, thereby affecting the measured radar backscatter coefficient [*Hosseinmostafa et al.*, 1995]; M. R. Drinkwater and V. Lytle (ERS 1 synthetic aperture radar and field-observed characteristics of austral fall freeze-up in the Weddell Sea, Antarctica, submitted to *Journal of Geophysical Research*, 1996) attribute a reduction in backscatter to the freezing of slush. In addition, *Drinkwater et al.* [1995] found that internal snow layers of different densities and snow volume scattering from thicker, old layered snow on second-year floes appear to be responsible for elevated backscattering on older ice floes. Thus changes in surface roughness (both snow and snow-ice interface), snow grain size and wetness, and/or melt-refreeze processes described in this paper account for a large dynamic range and the short-term variations noted in SAR backscatter at C band frequencies [*Drinkwater et al.*, 1993b]. For passive microwave measurements, *Lohanick* [1990, 1993] concludes that a snow cover often determines the absolute value and spatial variability of the observed brightness temperature; as such, it masks spatial variations in the surface properties of the underlying ice.

In spite of their significance, little is known about the interrelations and temporal evolution of the above processes, due to the sparsity of observations of temporal and spatial snow characteristics. Recent Antarctic field experiments have begun to make routine point estimates of snow thickness in conjunction with hourly ice observations, surface energy budget, modeling, and remote-sensing validation studies [e.g., *Ackley et al.*, 1992; *Allison et al.*, 1993; *Casarini and Massom*, 1987; *Casarini*, 1990; *Haas et al.*, 1992; *Jeffries et al.*, 1994a, b; *Lange and Eicken*, 1991; *Meese et al.*, 1990; *Wadhams et al.*, 1987; *Worby et al.*, 1994]. Few [e.g., *Eicken et al.*, 1994; *Sturm et al.*, 1996], however, have concentrated upon detailed analysis of snow conditions within a regional framework. In this paper we first describe observations of snow thickness, temperature, salinity, density, and stratigraphy and their variability carried out during voyage Ant X/4 of RV *Polarstern* [*Lemke*, 1994]. By means of measurements carried out on the same floe during a 3-day period when the ship was stationary, the temporal evolution of these properties is demonstrated. Finally, key observations made during this experiment are summarized.

2. Winter Weddell Gyre Study '92

The Winter Weddell Gyre Study '92 took place during the austral winter of 1992 [*Lemke*, 1994]. The ship entered the sea ice along the Greenwich meridian on June 12 (day 164) (Figure 1). At 70°S the course followed the Antarctic coastline southwestward before turning (on day 190) to traverse the central Weddell Sea ice pack and exiting from the pack to the north of King George Island (on July 29, day 211). The cruise track is divided into sectors, lettered A to E in Figure 1, which are roughly equivalent to specific ice regimes as presented by *Haas et al.* [1992] and *Drinkwater and Haas* [1994]. Each sector is summarized in Table 1. Entry into the marginal ice zone on day 164 (sector A) coincided with classic early-season pancake cycle growth [*Lange et al.*, 1989], whereas the approach to the ice edge and exit from the pack in the central northwest (D and E) coincided with an extreme rise in air temperature and storm activity, resulting in the large-scale melt of snow cover features consistently monitored further south.

2.1. Atmospheric Conditions

Hourly measurements of near-surface air temperature, wind velocity, wind direction, and atmospheric pressure collected onboard the ship are presented as time series in Figure 2. Stormy, mild periods typically alternated with calm, clear, and cold conditions over 3- to 5-day cycles, with the largest-

amplitude fluctuations in wind and temperature occurring within the marginal ice zone. Such fluctuations not only determine precipitation rates and snow thickness distributions but also drive strong snow metamorphism. A high proportion (78%) of average hourly wind speeds measured while within the pack exceeded 5 m s^{-1}, which is the approximate threshold above which saltation (i.e., wind transport) of unconsolidated snow begins [*Ackley et al.*, 1990]; 36% exceeded 10 m s^{-1} (Figure 2c).

At the time of the experiment, persistent strong winds were prevalent in the coastal sector B (Figure 1) and in the northwest (sectors D and E), with peaks in velocity and relative humidity accompanying winds from ~100° T and ~300° T, respectively, though over a large range. Whereas strong winds were typically accompanied in sector B by air temperatures of less than −10°C, those in the northwestern marginal ice zone were accompanied by temperatures exceeding −5°C (and even around 0°C), being associated with incursions of warm moist maritime air across the pack. Such conditions slow sea ice growth and can cause widespread surface melt. The overall effect of one such event on the regional snow cover, marked G in Figure 2, is described in section 4.2 and illustrated in meteorological images and passive microwave data by C. Oelke (Atmospheric signatures in sea-ice concentration estimates from passive microwave: Modelled and observed, submitted to *International Journal of Remote Sensing*, 1996).

2.2. Ice Conditions

Area-averaged values of the basic sea ice variables measured during the ship transit [*Haas et al.*, 1992] are presented in Table 2. These data concur with the conclusion of *Ficken et al.* [1994] that mean snow and ice thicknesses increase significantly to the west of 35°–40°W. They reflect the predominance of younger ice to the east and the outflow of older well-deformed ice to the west/northwest within a limb of the Weddell Gyre at the time of the experiment (June–July) [*Drinkwater et al.*, 1993b; *Massom*, 1992]. Routine ice observations collected in transit are summarized by *Haas et al.* [1992], together with photographs of the ice conditions, while in situ ice core and thickness measurements, together with shipborne radar backscatter data, are summarized by *Drinkwater and Haas* [1994].

Localized assemblages of thick (>5 m) high-freeboard floes (typically 50 m in diameter and with a snow cover of >1 m) were encountered in sector A; some are thought to represent broken-off fast or second-year ice [*Haas et al.*, 1992; *Wadhams et al.*, 1987]. Such floes were also observed in coastal sector B as far west as 70°S, 15°W, where they contributed up to 10% of the total ice concentration, and in sector E. They were generally avoided by the ship, and this study does not include samples from this ice type.

2.3. Snow Data Collection

Snow data were collected along the route shown in Figure 1. For analysis, data are split into (1) those collected remotely from the ship in transit and (2) those collected in situ during ice stations and by remote helicopter surveys. In transit data comprise snow (and ice) thicknesses measured routinely from the moving ship by monitoring ice floes overturned by the bow [*Haas et al.*, 1992]. For in situ data, 103 snow pits were excavated on a variety of ice types, ranging from undeformed young ice through deformed first-year to possible multiyear or fast ice. Of these, 31 were dug in association with ice core measurements [*Drinkwater and Haas*, 1994]; the remainder were made independently of ice samples.

Table 1. Ice Conditions Encountered in the Cruise Legs of the 1992 Winter Weddell Gyre Study

Sector	Dates	Primary Ice Types
A	June 13–18	diffuse ice edge, "pancake cycle," consolidating pancakes, nilas and grey ice, buildup of pressure near the Fimbul Ice Shelf front, localized swarms of high-freeboard thick floes (50–100 m in diameter with a 1-m-thick snow cover, e.g., June 18)
B	June 19 to July 8	refreezing coastal polynya, vast rubble fields along the ice shelf front, refreezing coastal polynya
C	July 9–13	alternating vast stretches of "stony fields"* and flat, uniform stretches of white ice with prominent sastrugi and "barchan dune" fields; large intermittent leads prominent; largely undeformed ice with a surface relief of <0.5 m
D	July 14–24	a band of mixed ice types: undeformed second-year (1.2–1.5 m thick), smooth medium-thick first-year (0.5–1.2 m thick), and highly deformed rough first-year ice (often >2 m thick); to the northwest, extensive lead systems covered in nilas
E	July 25–31	entry into this sector coincided with strong westerly winds, ice cover breakup, and a decrease in mean floe size; a band of thinner first-year ice with little or no snow cover, then a band of thicker undeformed second-year ice; heavy brash ice formation in the vicinity of the South Orkney Islands polynya; mosaic of melting floes, loosely aggregated floes, pancakes, and brash as the marginal ice zone was entered

*"Stony fields" refer to point-type roughness with associated sastrugi and snowdrifts, as described by *Wadhams et al.* [1987].

For the in situ data, vertical temperature profiles were recorded in 51 pits, and 90 pits yielded samples from various depths for grain size distribution analysis, salinity testing, snow classification, and macrophotography in the ship's coldroom. Samples were collected using standard 3-cm-high cutters with a volume of 100 cm^{-3}. No density samples were collected from pure ice layers, which were typically thinner than the snow sample cutters. Observations were also made of the presence/absence of flooding (slush) at the snow-ice interface, the clarity of the latter, and its roughness, stratigraphy, and snow surface roughness characteristics. Additionally, 441 in situ snow thickness measurements were collected, at a typical spacing of 1 to 2 m along 10- to 100-m transects, in association with ice thickness and freeboard level measurements, described in detail by *Drinkwater and Haas* [1994].

Certain limitations apply to the current snow data set. The ship was a moving observational platform, and regional/temporal variability cannot readily be determined as the data represent a series of "snapshots." It avoided very thick, heavily deformed ice. In situ samples were unevenly distributed in both space and time, with most being collected in sector D and

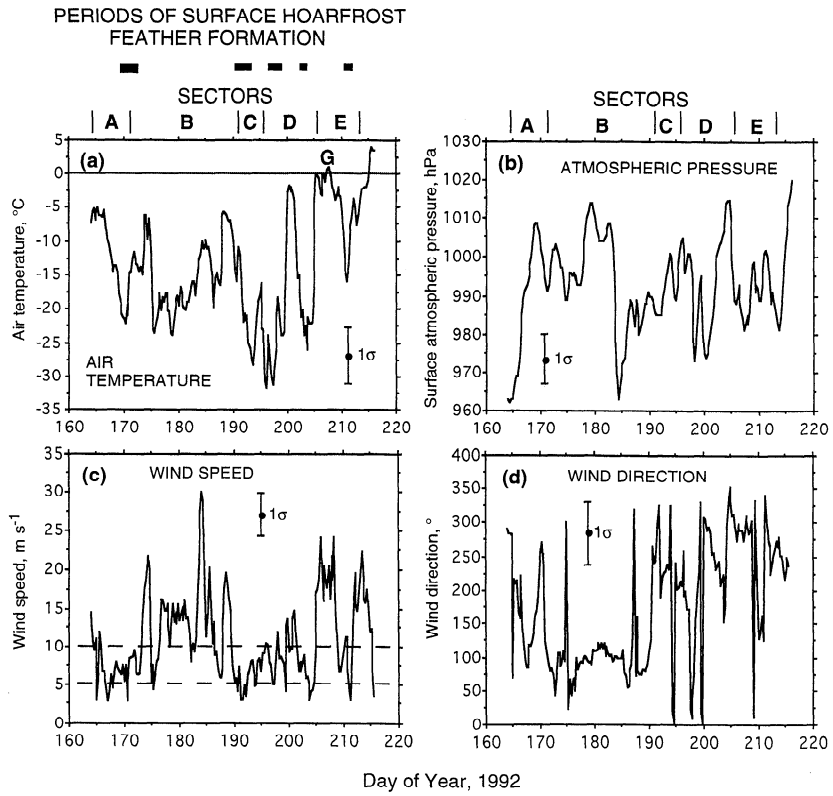

Figure 2. Time series of meteorological data (hourly observations) collected on the ship while within the pack: (a) air temperature, (b) atmospheric pressure, (c) wind speed, and (d) wind direction. Sectors from Figure 1 are marked, as are periods of surface hoarfrost formation.

confined to thicker ice types. An effort was made to alleviate sampling bias by choosing sample sites representative of the local snow cover. No $\delta^{18}O$ analysis was carried out on ice cores to determine the proportion of meteoric ice. Given these limitations, an assessment is made of broad-scale variability in snow thickness distribution, properties, and surface roughness characteristics. This data set is complemented by snow pit measurements carried out in the western Weddell Sea during the overlapping 1992 Ice Station Weddell Experiment [*Lytle and Ackley*, 1992].

3. Snow Characteristics

Interpretation of snow data collected over sea ice is complicated by the fact that it exhibits a high degree of variability in time and space in its properties and thickness distribution. In this section we examine snow characteristics on a variety of scales, from millimeter (grain size) to tens of meters (surface roughness).

3.1. Snow and Ice Thickness Distribution and Small-Scale Surface Roughness

Probability density functions (pdf's) for *in situ* and in transit snow and ice thickness data are presented in Figure 3. The overall mean snow depth measured in situ was 0.14 ± 0.17 m (i.e., $\pm 1\sigma$) and ranged from 0.00 to 0.95 m. Corresponding ice thickness measurements show a mean of 0.91 ± 0.64 m over a range of 0.05–6.00 m. In comparison, in transit snow depth measurements averaged 0.14 ± 0.15 m over a range of 0.0–1.0 m, with corresponding ice thicknesses averaging 0.67 ± 0.56 m over a range of 0.01–5.00 m. The modes of in situ (Figure 3a) and in transit (Figure 3b) snow data, which occur at 0.05–0.15 m, are largely associated with young and first-year ice. Secondary peaks around 0.50–0.65 m are associated with older ice, 2–3 m thick. Similarly, ice thickness pdf's are weakly bimodal, with distinct modes at 0.50–0.70 m in both in situ (Figure 3c) and in transit (Figure 3d) data; both tail off to local maxima at approximately 3 m and 2 m, respectively. That there are few measurements in lower thickness range for in situ and upper range for in transit is an artifact of biases associated with the sampling techniques.

Scatterplots of ice versus corresponding snow thickness from in situ and in transit measurements (with one outlier removed) are presented in Figures 4a and 4b, respectively. The relatively poor correlations (0.43 and 0.67) and large spread of points in both cases indicate that ice thickness cannot be accurately estimated from point measurements of snow thickness alone, particularly for deformed ice thicker than approximately 0.5 m (and late in the winter season). Due to wind-blown redistribution, thin snow is not exclusively associated with thin ice and vice versa; snow of less than 0.2 m and even 0.1 m thick is encountered on ice with thicknesses of greater than 1.5 m (Figure 4a). Better correspondence occurs for the in situ data when they are averaged for each transect (Figure 4c).

Effects of ice surface roughness perturbations on localized snow thickness are illustrated in Figure 5, with representative transect cross sections from level (Figure 5a), moderately deformed (Figure 5b), and moderately heavily deformed first-year ice (Figure 5c) [*Drinkwater and Haas*, 1994]. Even a minor surface perturbation such as at point A in Figure 5b can act like a snow fence, resulting in a localized deepening of the

snow cover. On flat ice surfaces, centimeter-scale snow surface roughness features initiate localized wind-blown accumulation. Such features form by the modification of nonprecipitated, surface hoarfrost feathers into icy nodule crusts. We term this process the "surface hoarfrost cycle." On cold, calm, clear nights, rapid kinetic growth of hoarfrost crystals, typically 1–3 cm in height, occurs by deposition of water vapor on a surface cooled to below the ambient air temperature by radiational cooling [*Colbeck*, 1991; *Lang et al.*, 1984]. Figure 2a indicates that periods of surface hoarfrost formation coincided with periods of low (but rising) air temperatures combined with mean wind speeds of <6 m s^{-1}. Such periods also coincided with frost flower formation on new ice forming in leads. Subsequent returns to warm, windy conditions lead to the formation of ice nodules on exposed raised centimeter-scale relief, by the enlargement, rounding, coalescing, and bonding of the original hoarfrost grains and underlying snow. Icy nodules, ranging in diameter from 0.2 to 0.8 cm, formed a continuous cover 0.5–1.0 cm thick on dune surfaces. Continued high air temperatures and humidity and windy conditions led to a coalescence of nodules along the crests and windward faces of these minidunes to form linear pure ice features commonly 1 cm wide, 1 cm high, and 3–10 cm long. With a return to cold clear calm conditions, the cycle repeats itself with a renewal of hoarfrost feather formation.

In the absence of ice deformation, such small-scale roughness features may act as foci for the formation of low, crescent-shaped dunes, which we term "barchans" due to their resemblance to the desert features. Extensive fields of barchans were encountered over the vast stretches of largely undeformed white ice in the central Weddell Sea (sector C). These features, which were typically 25 m across, 35 m long, and 0.5–1.0 m high and occurred at a spacing of approximately 5–10 m, resulted in a thickening by a factor of 1.5–3 compared to surrounding snow. Originally migratory, they develop a degree of semipermanency with age as crusts formed on their surfaces.

Where ice roughness is a factor, snow builds up in the lee of ridge sails and fills in gaps between sails, as illustrated in Figure 5c; snow thickness above sails themselves is minimal. Omnidirectional drifts are common due to floe rotation and/or changes in prevailing wind direction. Surface transect measurements show that sastrugi lead to an increase in snow thickness by a factor of 2–5 compared to adjacent regions; similar findings were reported by *Eicken et al.* [1995]. By aeolian redistribution, accumulating snow "smooths out" the ice surface roughness, thereby reducing the surface drag coefficient [*Andreas et al.*, 1993]. Angular sastrugi, with a typical elevation of 0.5–1.0 m, again become stabilized with time due to the formation of high-density surface crusts.

The in transit data are presented in Figure 6 as scatterplots of snow versus ice thickness for sectors A and E, which represent significantly different ice regimes, i.e., one encountered early in the cruise to the east and the other encountered 6 weeks later to the northwest. Snow and ice thicknesses are strongly correlated ($r = 0.8$) for new ice, formed under divergent conditions and carrying only recent accumulation. Such is the case for sector A (Figure 6a), which includes early "pancake cycle" growth in the marginal ice zone and nilas/grey ice formation further to the south. By comparison the scatter of points in sector E is large (Figure 6b). The low correlation between ice and snow thickness (0.39) reflects observed mixed fractions of aggregated floes with variable snow depth and an increase in surface melt, floe fragmentation, and brash ice formation as the marginal ice zone was approached and entered. First-year floes were characterized by rough surfaces with melt features, whereas second-year floes remained smoothed by snow up to 0.8 m thick.

Table 2. Mean Values for Sea Ice, Snow, and Meteorological Variables for Each of the Five Sectors Measured in Transit

	Region				
	A	B	C	D	E
Julian Day, 1992	164–170	171–190	191–195	196–206	207–213
Snow thickness, m					
Mean	0.04	0.10	0.11	0.16	0.35
Standard deviation	0.05	0.07	0.04	0.11	0.26
Minimum	0.0	0.01	0.02	0.01	0.00
Maximum	0.20	0.40	0.22	0.50	1.00
Ice thickness, m					
Mean	0.34	0.64	0.51	0.78	1.22
Standard deviation	0.31	0.39	0.15	0.32	0.99
Minimum	0.01	0.03	0.25	0.30	0.02
Maximum	1.50	2.00	1.00	2.00	5.00
Ice concentration, %					
Mean	88	97	99	99	77
Standard deviation	21.7	12.0	1.5	4.3	29.0
Minimum	0	10	90	70	1
Maximum	100	100	100	100	100
Floe size*					
Minimum	1	3	4	4	1
Maximum	6	6	6	6	6
Air temperature, °C					
Mean	−11.2	−16.1	−21.5	−18.4	−3.9
Standard deviation	5.9	3.6	5.2	9.5	4.0
Minimum	−22.7	−23.4	−31.7	−31.8	−16.2
Maximum	−4.3	−9.6	−10.9	−1.4	0.7
Wind speed, m s^{-1}					
Mean	6.4	9.7	6.3	8.6	14.1
Standard deviation	2.5	4.3	2.5	3.6	6.1
Minimum	1.5	2.3	2.3	1.6	0.4
Maximum	11.8	21	11.4	19.9	23.4
Wind direction, °T					
Mean	181	114	233	210	243
Standard deviation	77	65	72	94	80.0

*For floe size, 1, <1 m; 2, 1–3 m; 3, 3–10 m; 4, 10–100 m; 5, 100–1000 m; 6, >1000 m.

3.2. Snow Density, Grain Size, and Shape

Similar complexity was noted in snow properties as measured in snow pits. Seven broad categories of snow "type" were identified, based on the morphological (and process oriented) classification of terrestrial snow of *Colbeck et al.* [1990]. These represent new or recent snow, soft to moderately hard fine-grained (f.g.) layers, hard f.g. wind slab, depth hoar, icy layers/melt clusters, slush, and refrozen slush (although not strictly snow, the latter is referred to as "snow ice"). Typical snow covers comprise strata of widely differing thermal conductivities [*Sturm et al.*, 1997], with the complexity of assemblage being related to snow cover age (i.e., the number of precipitation events and length of metamorphism) which in turn is related to the age of the underlying ice. Mean grain size, density, and salinity for each class are given in Table 3a and for each sector in Table 3b. These reflect the degree of wind fragmentation and packing of grains, the duration and degree of metamorphism, and effects of wetting (both saline and nonsaline) and refreezing. Figure 7 presents relative frequency distributions from all measurements of snow type, density, salinity, and grain size.

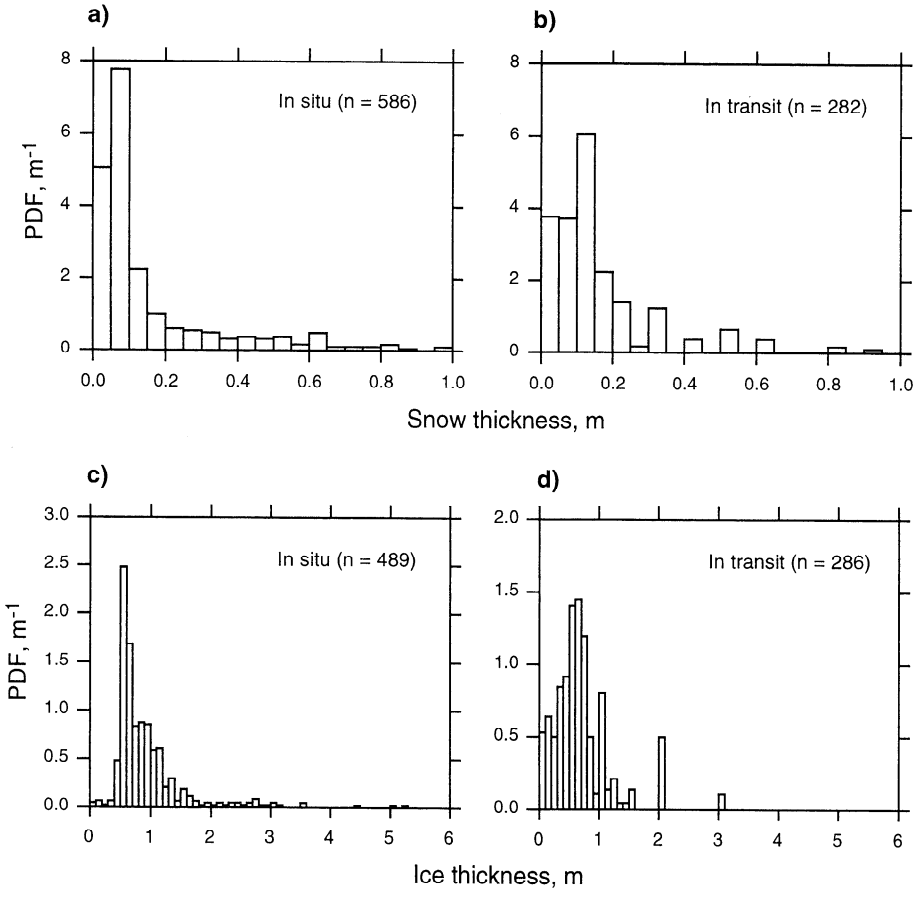

Figure 3. Probability density functions of total snow thickness data collected (a) in situ and (b) in transit and total ice thickness data collected (c) in situ and (d) in transit.

The mean overall density was 0.32 ± 0.09 g cm^{-3} (n = 132), ranging from 0.18 g cm^{-3} for large-flaked new snow to 0.67 g cm^{-3} for hard, well-bonded refrozen slush. The modal peak in Figure 7b occurs at 0.25–0.30 g cm ^{3}. The mean grain size was 2.73 ± 3.12 mm (n = 90) over the range of 0.2 mm for recent snow to 10 mm for well-developed depth hoar; refrozen slush cannot be readily described by grain size, as it typically forms a horizon of ice of polygonal granular texture (snow ice).

Whereas low-density new snow (0.18–0.21 g cm^{-3}) and soft to moderately packed, fine-grained snow (0.22–0.31 g cm^{-3}) were the primary snow types on newly forming pancake ice to the southeast (sectors A and B), substantial icy layers were present throughout sector E, comprising 7.6% of the total snow cover in 6 pits. Depth hoar was the prominent class in the northwest, as reflected in the larger grain size (Table 3b). Depth hoar/faceted crystals also formed the dominant snow class overall, accounting for 37% of the samples collected (Figure 7a). Although most depth hoar horizons sampled occurred at depth below buried crusts or icy layers, they were observed twice just below the snow surface (e.g., 10- to 20-mm grains in 0.65-m-deep snow on ice >2 m thick on July 17 at 64°57′S, 41°20′W). *Colbeck* [1989] suggests that near-surface depth hoar occurs as a result of the combined effects of the large variations in temperature and solar radiation at the surface and periodic fluctuations in near-surface temperature gradient.

3.3. Snow Stratigraphy

In this section we examine the stratigraphies of typical snow covers observed. Although they effectively represent "snapshots" and detailed analyses of process of formation cannot be carried out, they serve to illustrate the complexity and variability of the snow covering Antarctic sea ice. Figure 8a presents a profile of a typical thin (0.14 m) snow cover on July 19, on rafted 0.94-m-thick ice with little surface topography and a freeboard of +0.06 m. The basal substrate consisted of rounded grains, 0.5–1.0 mm in diameter, with a density of 0.37 g cm^{-3}. The salinity of 14‰ suggests that this basal layer was at some stage damp, probably as a result of upward brine rejection during ice growth. This layer was overlain by low-density (0.20 g cm^{-3}) consolidated depth hoar comprising grains up to 8 mm in diameter. Above this a typical hard fine-grained wind slab (with a density of 0.26 g cm^{-3}) was capped with a forming 0.5-cm-thick icy crust.

In contrast, Figure 8b presents a stratigraphic profile of a 0.84-m-deep snow pit on a high-freeboard, thick (>3.5 m) second-year floe typical of the northwestern Weddell Sea. Grain size is uniformly large (1–4 mm), with a large proportion of depth hoar (both fully developed and weakly bonded and with rounding and sintering). Unlike the thinner stratigraphy a significant proportion of the vertical profile (9.5%) comprises four icy layers, reflecting cyclical melt-freeze activity (see section 4.2 for a description of one such episode). Buried crusts

form the focal point for lateral ice accretion as meltwater penetrates the snow cover via percolation channels [*Colbeck*, 1982]. Resultant clear "plate glass" ice horizons up to 3 cm thick were observed on a number of occasions in sector E. Such dense icy strata are characterized by a high thermal conductivity compared to lower-density snow [*Sturm et al.*, 1997], sharply reducing the temperature gradient in that layer and thus increasing the temperature gradient through the more permeable layer. *Colbeck* [1991] surmises that such conditions decelerate vapor flow immediately below the layer, often leading to enhanced rapid grain growth which is associated with the higher supersaturation [*Moore*, 1982]. With time, hardened horizons in dry snow covers may be replaced by depth hoar due to large persistent temperature gradients [*Colbeck*, 1991].

Further evidence of periodic melt was available at the snow base, where rounded nodules of ice, typically 0.06 m high and 0.15 m in diameter, protruded from the ice surface. Such features are related to the downward migration of free water through the snow mass along percolation columns, with the water spreading out along the sea ice surface and refreezing. Where the vertical percolation columns refreeze, they form "ice pipes."

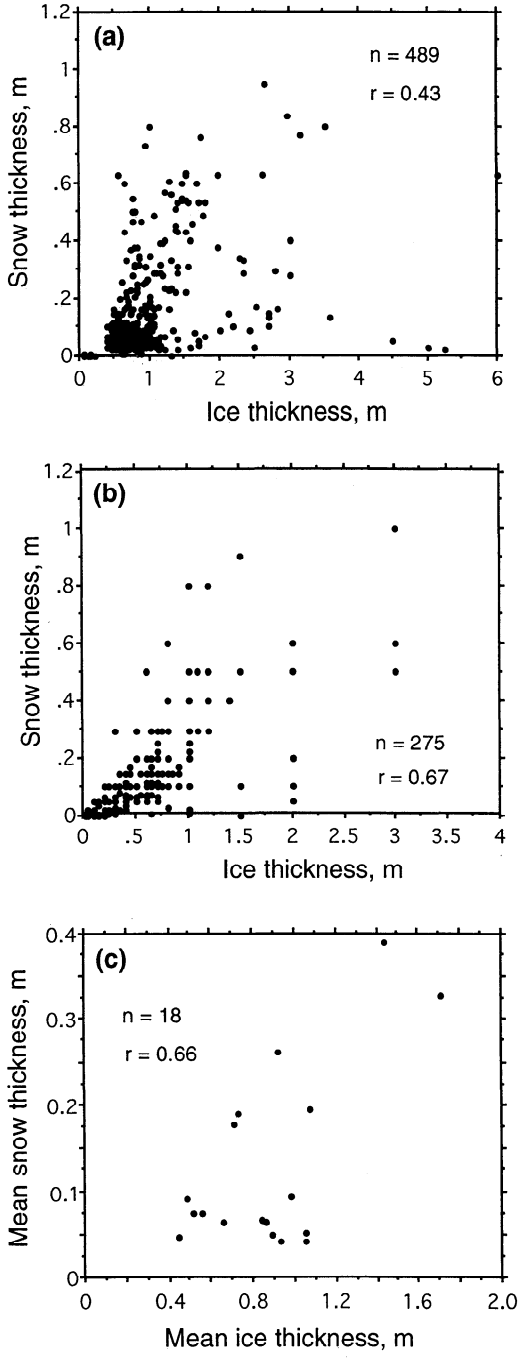

Figure 4. Scatterplots of sea ice versus snow cover thickness for total data collected (a) in situ and (b) in transit and (c) for mean ice versus snow thickness along in situ thickness transects.

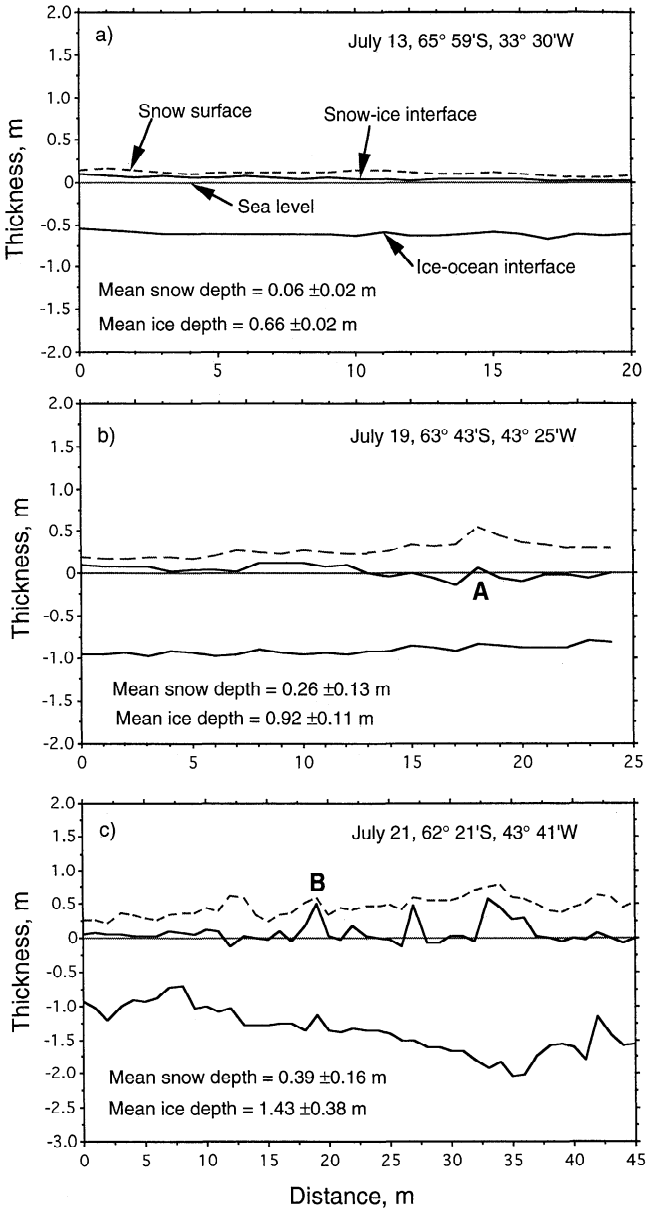

Figure 5. Snow and ice thickness transects from typical first-year ice surfaces: (a) flat, even ice (sector C), (b) moderately deformed ice (sector D), and (c) moderately heavily deformed ice (sector D). The dotted line at zero thickness denotes sea level, i.e., zero freeboard. Note that the scales are different.

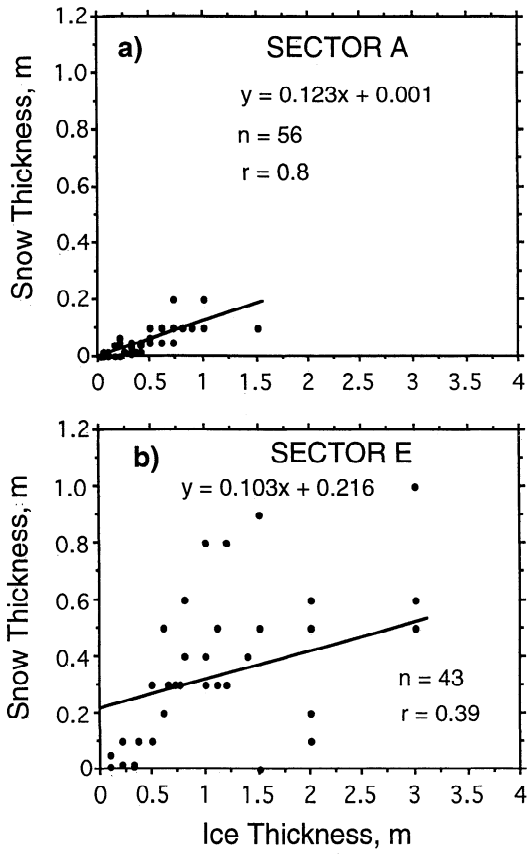

Figure 6. Scatterplots of sea ice versus snow cover thickness for data collected in transit from the ship for (a) sector A and (b) sector E.

3.4. Snow Salinity

The mean observed overall snow salinity was 8.68 ± 10.7‰ over a range of 0.0–48.0‰ (n = 189) (Figure 7c), with the modal salinity falling between 0 and 5‰. Mean salinities for each of the sectors, apart from A, are presented in Table 3b. The plot of salinity versus height within the snow column (Figure 9a), based upon 141 samples from 37 snow pits, shows that snow salinity comprises two components: (1) a "background" salinity of <1‰ in the upper part of the snow column, likely contributed by blowing snow which has wicked salt or input of aerosol or sea spray transported salt during strong winds over adjacent leads and polynyas, and (2) a high- (>10‰) salinity basal component, often damp. Figure 9b presents salinities derived from ice surface scrapes versus ice thickness. Though representing a limited data set, a negative correlation (r = −0.80) exists between ice thickness (related to age) and ice surface salinity. Figure 9c, the salinity of the snow basal layer (0–0.03 m above the snow-ice interface) versus snow thickness, suggests that basal salinities exceeding 10‰ commonly occur under relatively thin snow covers, less than 0.15 m thick, on newer ice forms (grey-white to white ice) which had likely never flooded due to snow depression. Two outliers denote sites of slush formation under thick snow. Results suggest that even though newer ice forms have a positive freeboard, brine is available at their surface for vertical uptake into an accumulating snow cover. Possible mechanisms for snow salination are examined in section 4.3.

Table 3a. Mean Snow Grain Size, Density, and Salinity as They Relate to Snow Type

Snow Type	Grain Size, mm		Density, g cm^{-3}		Salinity, ‰	
	Mean	σ	Mean	σ	Mean	σ
New	0.8	0.4	0.2	0.03	4.8	11.6
Soft and moderate						
Fine-grained slab	1.2	1.8	0.3	0.04	5.7	7.6
Hard fine-grained slab	1.0	1.0	0.4	0.06	3.8	5.8
Depth hoar	4.9	3.5	0.3	0.08	7.5	8.3
Slush	...	...	...	...	26.3	6.1
Refrozen slush*	...	...	...	...	20.1	14.8
Ice surface scrape	...	...	...	...	22.8	12.0

*The refrozen slush (snow ice) salinities are based on three measurements only.

Table 3b. Mean Snow Grain Size, Density, and Salinity for Each of the Sectors in Figure 1 (Apart From Sector A)

Sector	Grain Size, mm		Density, g cm^{-3}		Salinity, ‰	
	Mean	σ	Mean	σ	Mean	σ
B	0.3	0.1	0.3	0.07	8.7	11.7
C	1.7	1.6	0.3	0.66	16.5	12.6
D	3.1	3.3	0.3	0.09	7.6	9.2
E	2.8	1.4	0.4	0.07	1.4	0.9

4. Discussion

4.1. Snow Metamorphism and Conductive Heat Flux

Colbeck [1982] shows that faceted growth forms occur at the expense of rounded forms when the localized temperature gradient is large (at least −0.1 to −0.2°C cm^{-1}). Here we define snow temperature gradient as $(T_s - T_i)/z_s$, where T_s is the temperature of the snow surface, T_i is that of the snow-ice interface, and Z_s is the snow thickness. For z_s we define zero as the snow-ice interface; thus a negative temperature gradient would occur where $T_i > T_s$. Temperature gradients of ≥−0.2°C cm^{-1} were observed in 69% of the pits measured. Figure 10 shows the relationship between snow thickness and temperature gradient based upon snapshot samples. Not surprisingly, large temperature gradients (to −2.0°C cm^{-1}) typically occurred in snow covers thinner than approximately 0.25 m. Although gradients dropped off significantly in thicker snow covers, they remained at approximately 0.2°C cm^{-1} to a snow thickness of about 0.6 m. The effect of high-temperature gradient metamorphism is reflected in the overall grain size distribution, with 48% of samples exceeding 2 mm in diameter (Figure 7d).

That vertical thermal gradients constantly adjust to synoptic atmospheric variability is illustrated in Figure 11. Temperature gradients in snow covers of similar depth but from different locations are compared with air temperatures over a 15-day period (July 15–30). Cyclical high-amplitude changes in air temperature take a relatively long time to penetrate to the snow-ice interface beneath thick snow covers. Much of the gradient in this example is contained within the uppermost 0.2 m of snow. Thus the difference in snow surface temperature between, for example, days 196 and 206 (July 15 and 24) is +23°C, compared to that at a depth of 0.48 m of approximately

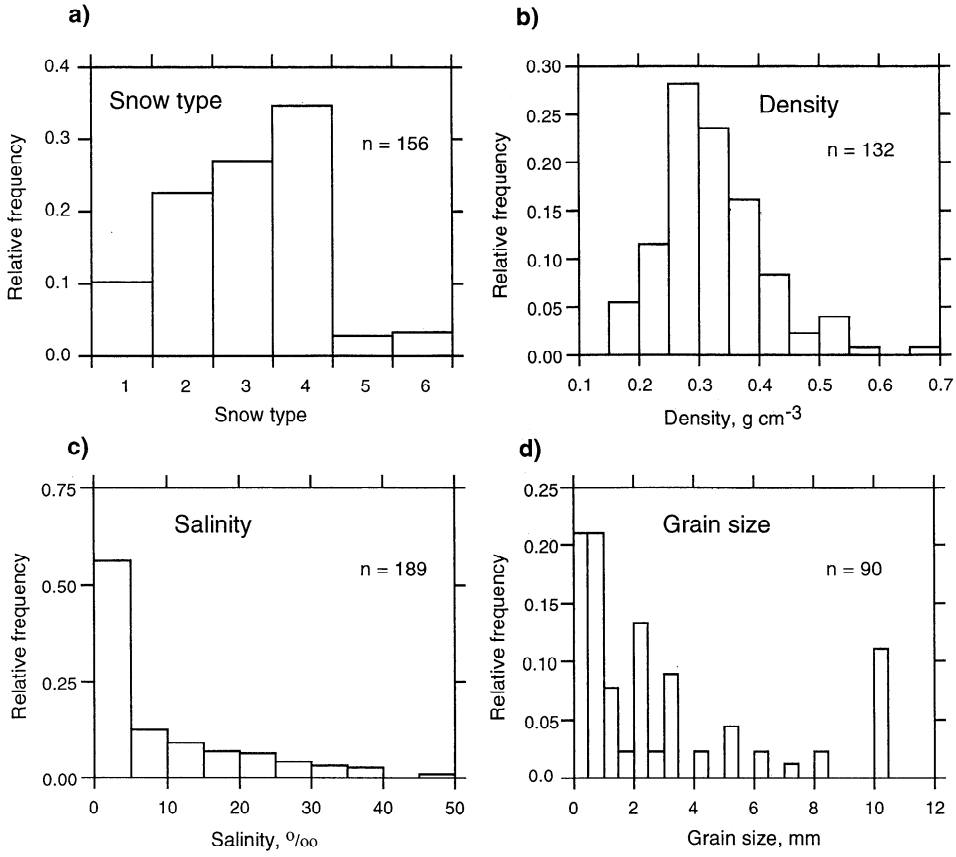

Figure 7. Relative frequency distributions of total in situ measurements of (a) snow type, (b) snow density, (c) snow salinity, and (d) snow mean grain size. In Figure 7a the numbers indicate 1, new snow; 2, soft to moderately hard fine-grained slab; 3, hard fine-grained wind slab; 4, depth hoar; 5, slush; 6, refrozen slush ("snow ice"). Icy layers were encountered in sectors D and E but were not sampled (see section 3.2).

+5°C in response to an increase in air temperature of +25°C. As thermal waves penetrate from above, so C- and S-shaped profiles are established, the largest gradients of which are associated with the lowest air temperatures.

From *Jordan* [1991] the thermal conductivity of snow, k_s, is estimated as

$$k_s = k_a + (7.75 \times 10^{-5}\rho_s + 1.105 \times 10^{-6}\rho_s^2)(k_i - k_a) \quad (1)$$

where k_a is the thermal conductivity of air (0.023 W m^{-1} K^{-1}), k_i is that of pure ice (2.29 W m^{-1} K^{-1}), and ρ_s is snow density. If a mean bulk snow thermal conductivity of 0.15 W m^{-1} K^{-1} were used, which is typical for snow densities in the range 0.2–0.3 g cm^{-3} [*Sturm et al.*, 1997], then we obtain the range of conductive heat flux (F_a) indicated on the right axis in Figure 10. The formulation used here is that of *Yen* [1981]:

$$F_a = -k_s(\partial T/\partial z_s) \quad (2)$$

where ∂T is the difference in temperature between the snow-ice interface and the snow surface and z_s is the snow thickness. Thus, for a mean temperature gradient of -1.0°C cm^{-1}, for example, the typical conductive heat flux through the snow layer is of the order of 15 W m^{-2}; most points lie beneath the threshold of $\pm$15 W m^{-2}. These values are derived assuming a linear temperature gradient, which is a reasonable approximation for thin snow. For thicker snow, however, nonlinear temperature gradients are more the norm; a temperature gradient which is strongly negative at the base but positive near the top will, for example, lead to a different conductive heat flux.

Sturm [1991] reported that depth hoar is characterized by a very low thermal conductivity. This implies that thermal gradients help preserve the warmer basal temperatures by generating kinetic grain growth forms, thereby further reducing the thermal conductivity of the snow layer and giving rise to a large temperature gradient at a given heat flow. This in turn drives rapid grain growth and desintering, further reducing the thermal conductivity. This positive feedback mechanism regulates conductive heat loss and gain. Detailed measurements of changes in the surface energy budget in response to the changing atmospheric variables during the 3-day station are presented by *Drinkwater* [1995].

4.2. Effect of Extreme Variability in Atmospheric Forcing on Snow Metamorphism

Cyclical synoptic-scale variability in atmospheric parameters has a significant effect on snow covering Antarctic sea ice, even in winter. In this section we present the effects of one such episode, observed during a 3-day station (July 21–24, 1992). Initially, the air temperature rose by 22°C in 12 hours as a deep low-pressure system passed over the experimental site (Figure 12). In response the snow temperature gradient reversed from negative to positive (Figure 13).

Prior to the rapid rise in air temperature, the snow was composed of three layers and spatially uniform. The basal layer

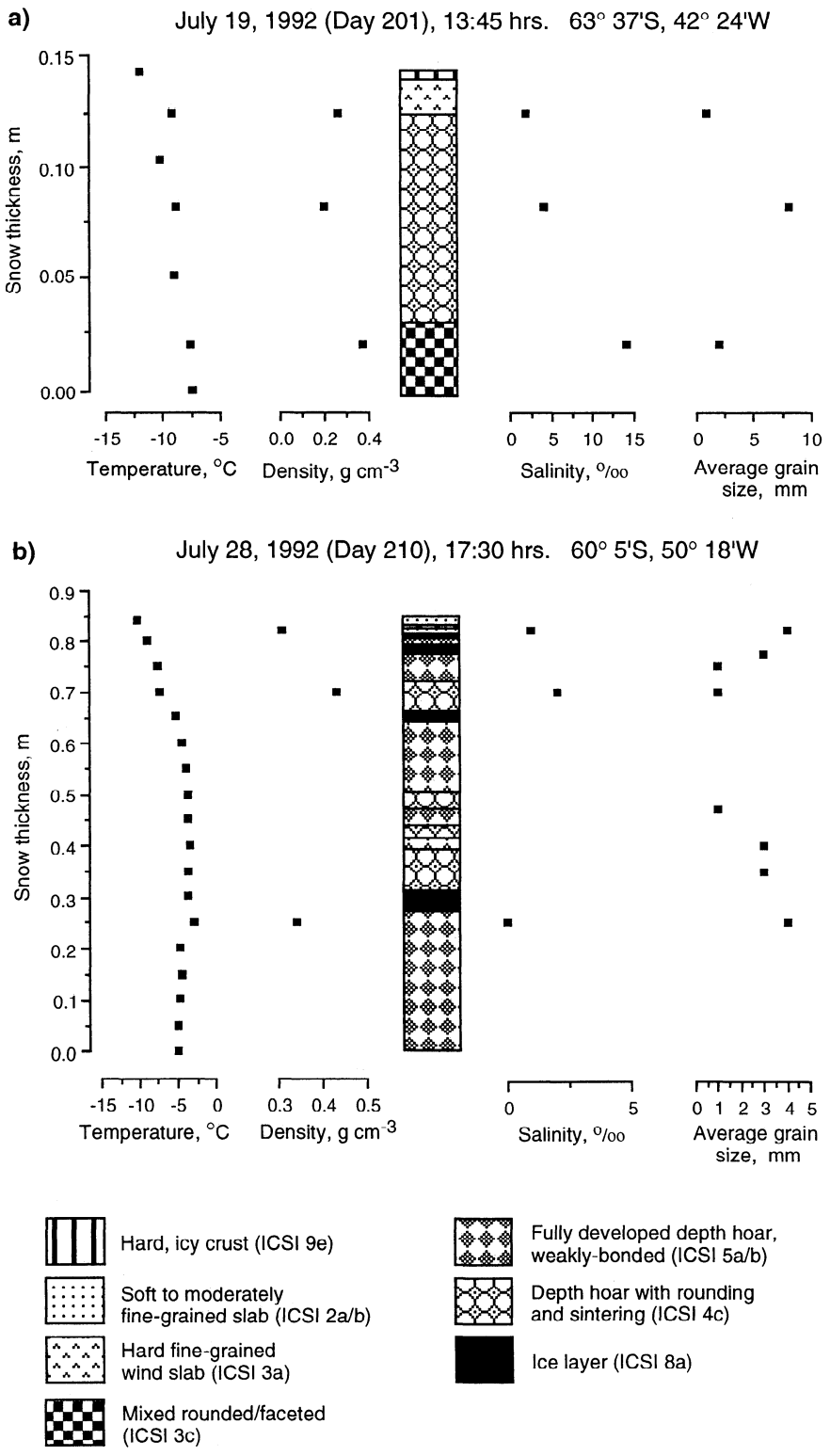

Figure 8. Typical stratigraphic profiles for (a) thin, relatively new and (b) thick, relatively old snow covers. For density, salinity, and grain size the squares represent the center points of 3-cm-high samples. ICSI refers to the snow classification of the International Commission on Snow and Ice [*Colbeck et al.*, 1990].

comprised saline (8–20‰) depth hoar with a density of 0.3 g cm^{-3} and mean grain size of 1 mm. Above this layer was a densely packed stratum of fine, wind-blown crystals with clusters of sintered, angular stellar fragments; this layer had a density of around 0.4 g cm^{-3} and a typical background salinity of <1‰. On top was a 0.5-cm-thick dense surface crust, which at the outset was carpeted in hoarfrost feathers.

By July 23, significant surface warming had occurred, with an increase in snow temperature leading to a reduction in temperature gradient. Rapid grain growth ceased, and facet

rounding and sintering occurred in the manner described by *Colbeck* [1982]. Twelve hours later, and after a period of damp snowfall, air temperatures of about 0°C and wind speeds of >15 m s^{-1} were accompanied by a low cloud base (around 1000 feet (304.8 m)) and high humidity, leading to melt and condensation at the surface (at approximately point Y in Figure 12). Rapid surface crustal formation followed, with icy nodules 0.2 cm in diameter embedded in a matrix of granular snow. The brief cloud-free cooling at point R combined with a reduction in humidity to encourage refreezing of moisture in the snow layer. Moisture reappeared in the snow with the subsequent rise in air temperatures to approximately zero and the reappearance of longwave radiation-trapping low cloud cover. Surface icy nodules grew to 0.5–0.7 cm in size, forming a high-density crust with an uneven microrelief (with elevations up to 1 cm). Nodules progressively coalesced to form rows of ice 1–2 cm wide and 2–6 cm long, particularly along exposed ripple crests (which covered the whole surface). The effects of these transformations on radar backscatter are discussed in detail by *Drinkwater et al.* [1995].

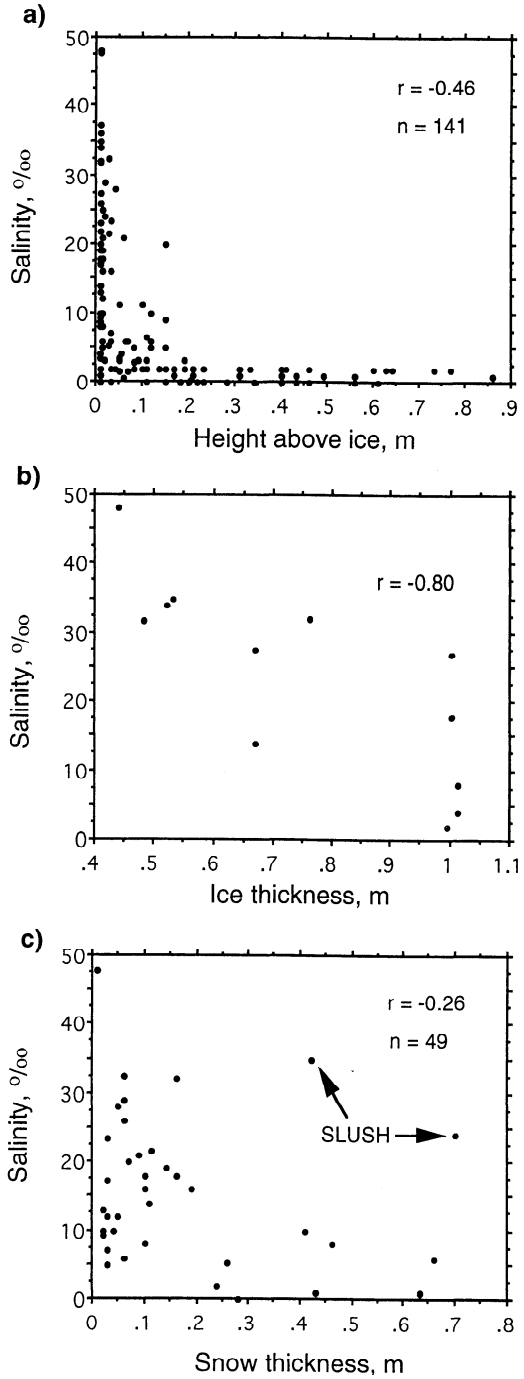

Figure 9. Scatterplots of (a) snow salinity versus height above the ice surface within the snow column, (b) ice surface scrape salinity versus ice thickness, and (c) snow basal salinity versus snow thickness.

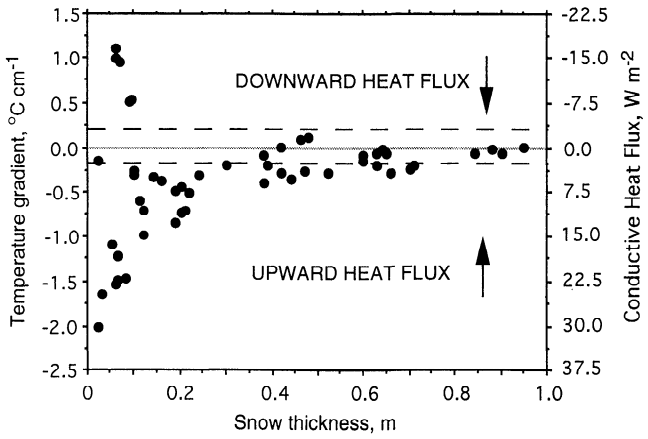

Figure 10. Scatterplot of snow temperature gradient and conductive heat flux versus snow depth (n = 53). The dashed lines denote the approximate threshold above which crystal faceting occurs in dry low-density snow [*Colbeck*, 1982].

The overall effect of this 2- to 3-day melt event was to produce a diffuse and fragmented ice cover, estimated at 70–75% concentration in the region of 61°00′S, 42°58′W (July 25). Snow surfaces became wet, with little or no snow redistribution or wind drift taking place in spite of the strong winds. By midday of July 25, snowfall had turned to rain then sleet (at 60°55′S, 43°01′W). Surviving fragments of flat floes, remnants of the vast regions of undeformed ice noted earlier, were melt affected (e.g., at 60°24′S, 46°34′W on July 26). Exposed to high temperatures and rain/sleet, all shallow areas of "unconsolidated" (low density) snow had melted away to expose the underlying sea ice, pitted and pock marked on a centimeter scale and grey (i.e., a significant change in albedo). The only regions of snow to survive were hardened crescent-shaped barchan dunes. In the intervening areas, domed pedestals of glazed snow, 0.20–2 m across and 0.03–0.04 m thick, occurred, raised up to 0.06 m off the slushy ice surface on thin icy supports. Thicker snow covers on the high-freeboard floes noted earlier also generally survived these destructive conditions. The subsequent drop in air temperature (from point O onward in Figure 11) and clearing of skies associated with a rise in pressure and a decrease in wind speed caused refreezing of the residual snow and wet ice surfaces. Surface observations on July 26 revealed that the flat white-ice floes, recently stripped of their snow cover, were covered in grey melt features and had a surface crust of ice 2 cm thick covering 10 cm of slush.

4.3. Mechanisms for Snow Salinization

In this section we assess possible mechanisms for snow salinization, none of which are mutually exclusive. Previous work [e.g., *Ackley et al.*, 1990; *Eicken et al.*, 1994; *Lange et al.*, 1990;

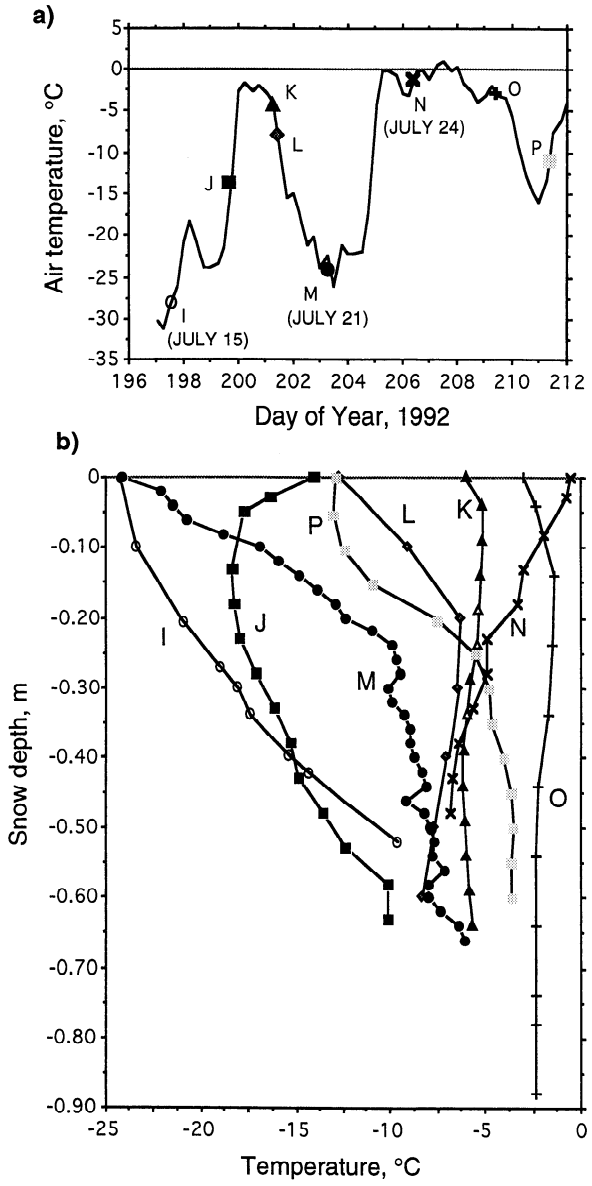

Figure 11. Time series of (a) surface air temperature and (b) snow cover temperature in eight vertical profiles of equivalent thickness over the period July 15 (day 197) to July 29 (day 211), 1992. The lettered points in Figure 11a correspond to the lettered profiles in Figure 11b.

Wadhams et al., 1987] has considered flooding quantitatively largely as a result of snow loading. Of snow samples collected from a height of 0–3 cm above the ice surface, 90% had salinities of >5‰, with a mean of 16.2 ± 11.3‰ over a range of 0.5–47.8‰. Similar observations have been made elsewhere [*Sturm et al.*, 1996; *Jeffries et al.*, 1994a].

In order to evaluate the prevalence of flooding, ice freeboard versus the ratio of snow to ice thickness is plotted in Figure 14a, derived from point measurements (from core, snow pit, and thickness transects combined), with corresponding means from the 18 in situ transects in Figure 14b. Of the 468 measurements over a wide range of ice and snow thicknesses, 8% had a negative freeboard and 3.5% a zero freeboard, with the majority of these occuring in sector D. The mean freeboard was 0.06 ± 0.08 m, and, significantly, 42% of the data fell between zero and +0.05 m freeboard and 75% between zero and +0.10 m. Thus the potential exists for further flooding in response to minor changes in sea ice isostatic balance, should channels be available between ice surface and ocean.

Following *Ackley et al.* [1990] and *Eicken et al.* [1994], the isostatic balance equation for undeformed sea ice floating on seawater is

$$\rho_w d = \rho_i(f + d) + \rho_s z_s \tag{3}$$

where ρ_w is the density of seawater (1.03 g cm^{-3}), d is the sea ice draft, ρ_i is the density of sea ice (assumed 0.90 g cm^{-3}), f is the sea ice freeboard, ρ_s is the snow density, and z_s is the snow thickness. For flooding to occur on an undeformed sheet of ice, $f = 0$ or $z_i \leq d$, where z_i is the ice thickness. Solving (3) for the ratio of snow to ice thickness z_s/z_i, where $z_i = d$ for potential flooding to occur, we obtain

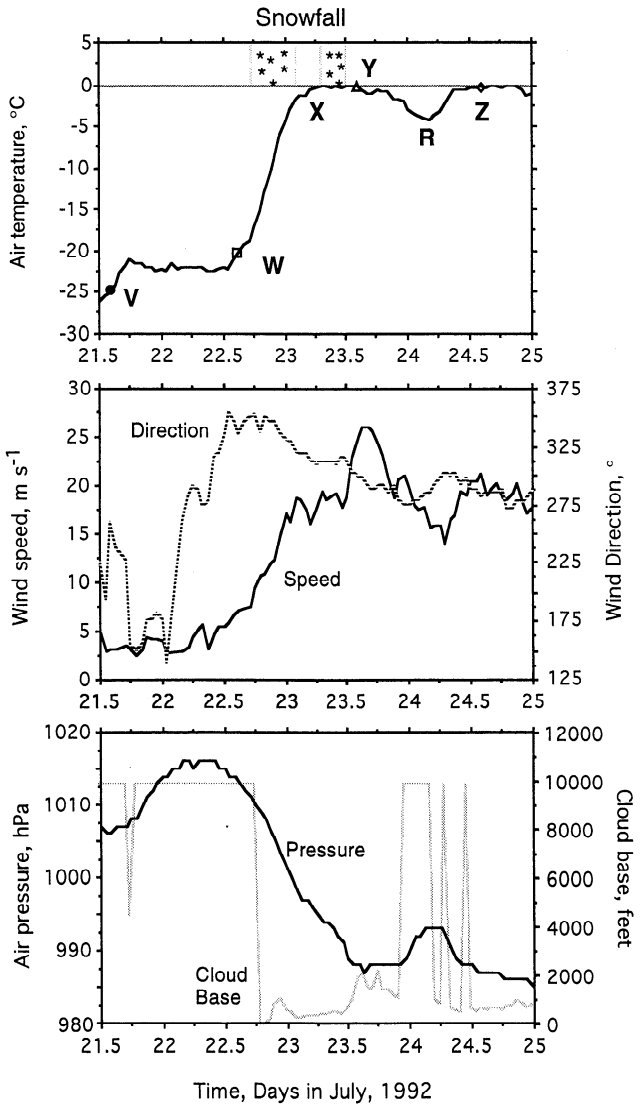

Figure 12. Time series of near-surface meteorological variables measured from the ship while stationary during the ice station of July 21–25, 1992. Snowfall events are marked at the top. The letters V, W, Y, and Z correspond to temperature gradients in Figure 13.

$$z_s/z_i \geq (\rho_w - \rho_i)/\rho_s \quad (4)$$

If ρ_s = 0.32 g cm ^{3} (i.e., mean snow density), the critical threshold ratio of z_s/z_i above which flooding would occur is 0.41. Thus 0.21 m of snow would be required to induce potential flooding on a level sheet of ice 0.5 m thick. Arrowed markings along the top of Figure 14a refer to snow densities which would be required to induce flooding (i.e., zero or negative freeboards) at the corresponding ratios of snow thickness/ice thickness.

The regression line in Figure 14a intercepts the zero freeboard at a snow/ice thickness of approximately 0.34, which is close to the critical threshold described above. A significant proportion (92%) of the observed data falls below this threshold. Closer examination of the remaining 8% of data at and above the critical threshold reveals that all originate after July 10 from the middle of sector C to sector E, with a high proportion occurring on July 19–22 to the southeast of the South Orkney Islands. They occur on thicker ice (mean 1.04 ± 0.36 m) with a mean snow cover of 0.47 ± 0.14 m.

In the present study the highest range in freeboard (−0.05 to +0.6 m) occurs before the snow/ice thickness ratio reaches 0.2 (Figure 14a): within this range, some zero and negative freeboards are noted at ratios between 0.13 and 0.25. In these cases, bulk snow densities exceeding 0.5 g cm^{-3} would be required to upset the isostatic balance. Such conditions are not satisfied by observed regional mean snow densities (Table 3b). This implies that while snow loading is an important mechanism for inducing flooding and snow-ice formation, other processes, related to ice deformation, are also responsible for flooding of the snow-ice interface and may be regionally as important.

In Figure 14b, only one point corresponds to a mean negative freeboard, and the correlation between mean freeboard and snow/ice thickness is −0.68. The corresponding correlation for the total point measurements in Figure 14a is −0.32. Drilled thickness transects of closely spaced thickness holes (Figures 5b and 5c) reveal that on a given floe, negative freeboards tend to be discontinuous and closely associated with ice depression around ridges. Subsequent snow drifting compounds the depression.

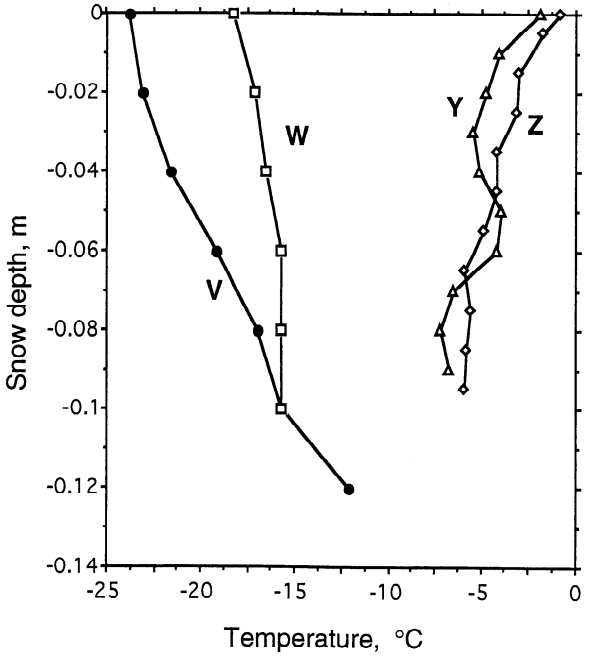

Figure 13. Time series of vertical temperature profiles in shallow snow during the ice station of July 21–25, 1992. The letters V, W, Y, and Z correspond to times as marked on Figure 12.

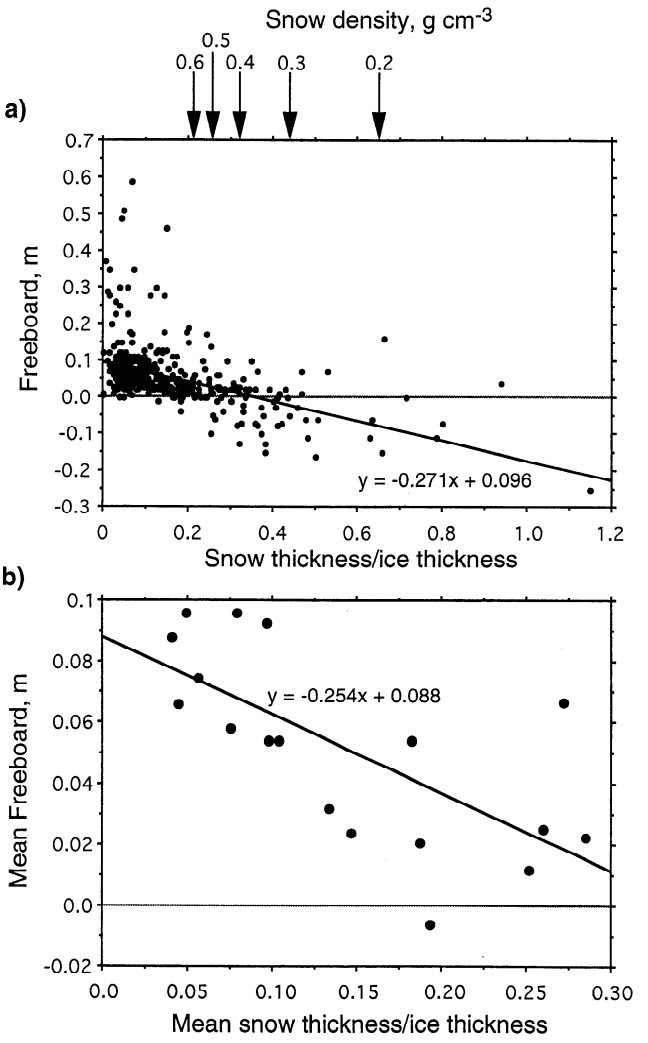

Figure 14. Scatterplots of (a) snow thickness/ice thickness versus freeboard for the total in situ measurements and (b) mean measurements along transects, derived from Figure 14a. Arrowed markings along the top refer to the critical threshold points along the snow thickness/ice thickness axis above which snow of a given density will depress an undeformed ice surface to, at, or below sea level. Snow with a density of 0.1 g cm^{-3} will cause depression when the snow/ice thickness ratio is ≥1.3.

That the equations for both regression fits in Figures 14a and 14b are so similar implies that an average (bulk) snow density can be calculated if the freeboard and snow and ice thicknesses are known, assuming that the ice is undeformed. Combining the regression fits with (4), snow density values of 0.37 and 0.38 g cm^{-3} are required to cause negative freeboards with the point and mean transect measurements, respectively. This compares with a measured overall average snow density of 0.32 g cm^{-3}.

Figure 15 presents the proportion of zero and negative freeboards combined observed along in situ snow/ice thickness transects (measurement spacings 1–2 m) as a function of time.

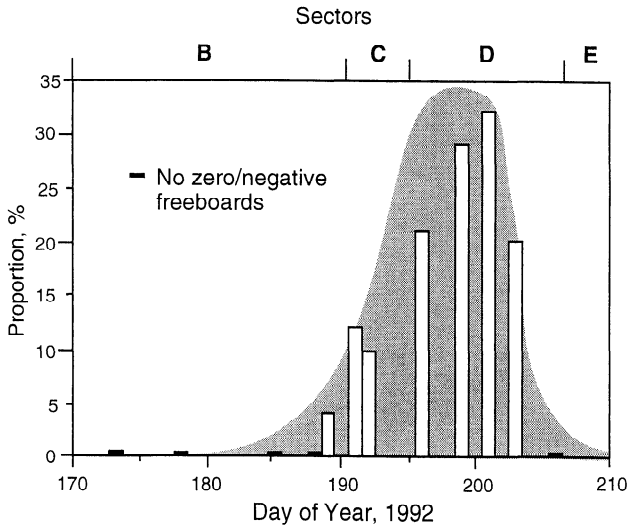

Figure 15. The proportion of zero and negative freeboards combined, observed along in situ snow/ice thickness transects (measurement spacings 1–2 m) as a function of time.

Negative freeboards were first observed in sector C, peaking at the midpoint of sector D. Negative freeboards were also encountered at four core sites from day 209 to 211 in sector E. The relative lack of negative freeboards to the east (in sectors A, B, and C) may be related to the earliness in the ice growth season, with the ice being of insufficient age to accumulate sufficient snow to cause loading. The exception is evidently heavy snow accumulation on newly forming thin ice which is still relatively permeable; unfortunately, we have few data from ice <0.1 m thick.

In dynamic marginal ice zones and adjacent to large leads and polynyas (such as the South Orkney Islands polynya), wave and swell overwashing are also an important cause of flooding. In addition, floe fracturing and rubble buildup by wave and swell action, and at times melting from below [*Lytle and Ackley*, 1996], set up an isostatic imbalance on individual floes, leading to negative freeboards and saline surface pond formation. Pond features, typically 1–5 m across, were observed mainly from July 26 onward (from ~60°S, ~46°W), in places covering 5–10% of the floe surface area. Such ponds, which may subsequently refreeze and become snow covered, were also noted during the 1986 Winter Weddell Sea Project cruise [*Wadhams et al.*, 1987].

Salination of the basal snow can occur in the absence of flooding. Observations suggest that the "wicking" of brine from the ice surface by capillary suction by newly fallen snow is an important process for incorporating brine into snow on newer ice types. Brine extruded onto the surface of nilas as a thin skim [*Perovich and Richter-Menge*, 1994] is quickly adsorbed by new snow or frost flower crystals [*Drinkwater and Crocker*, 1988]. This source term diminishes as the ice ages (thickens) and acquires a snow cover. Frost flower formation on dark/light nilas was widespread, under cold, clear, and calm conditions, similar to those required for hoarfrost feather formation (see Figure 11a). On June 17, for example, a salinity of 47.8‰ was measured in 1-cm-thick new snow on growing light nilas, as highly saline frost flowers were covered by a freshly fallen snow cover.

Conversely, low snow salinities were observed almost exclusively in older snow covers on thicker ice, likely due to the original salt content becoming redistributed within the snow or diluted by desalination. For example, a 0.62-m-deep snow cover on a thick second-year floe, at 64°57'S, 41°19'W on July 17, had a basal salinity of only 1.0‰. Snow crystal characteristics and the degree of grain bonding in these basal strata suggest that percolation of meltwater from above and subsequent refreezing played a key role in altering snowpack morphology.

5. Conclusions

Due to the complexity of conditions present (mixing) and limitations in the sampling strategy, which represented a series of snapshots along a cruise track, it is difficult to draw detailed conclusions about possible temporal and spatial relationships observed in the data. Given this limitation, significant variability is noted in both snow thickness and properties. The mean observed snow thickness for Winter Weddell Gyre Study (WWGS) '92 of 0.14 ± 0.17 m compares to 0.26 ± 0.23 m for the WWGS '89 study along a similar transect in September–October 1989 [*Eicken et al.*, 1994]. The larger value for the latter likely reflects the different season and longer snow accumulation time but may also be a function of interannual and regional variability in precipitation patterns (although few data are available to conclusively test this).

Although separated by a period of 5–7 weeks, substantial differences exist between mean snow thicknesses observed in the east and in the northwest, i.e., 0.07 m versus 0.35 m. Routine hourly ice observations concurred with earlier ones by *Lange and Eicken* [1991], showing that the pack of the northwestern Weddell Sea contained a significant proportion of older ice, consisting of thick first-year and second-year ice outflowing from the Weddell embayment in the western limb of the Weddell Gyre (as identified in enhanced-resolution ERS 1 scatterometer data by *Drinkwater et al.* [1993b] and passive microwave data by *Massom* [1992]). The region of perennial ice formation in the southwest corresponds with the zonal (>70°S) and seasonal (February–April) snow precipitation maxima [*Eicken et al.*, 1994]. At the time of observation the ice cover in the east consisted largely of new ice formed by the classic "pancake cycle."

Due to the magnitude and persistence of winds both during and after snowfall, snow redistribution is a key factor affecting both the snow thickness distribution (through localized erosion and buildup) and the amount of direct precipitation and snow "loss" via leads into the ocean. This finding is consistent with those of previous wintertime experiments in the region (e.g., the Winter Weddell Sea Project of 1986 [*Wadhams et al.*, 1987]) and elsewhere in Antarctica [*Sturm et al.*, 1996]. Snow thickness distribution within a given ice regime is closely related to the age, meteorological history, and degree of deformation within that regime [*Lange and Eicken*, 1991]. However, although point ice roughness features such as ridge sails form the focus for enhanced wind-blown accumulation in the form of sastrugi, fields of "barchan" dunes also have a significant effect on the snow thickness distribution on large expanses of relatively flat, largely undeformed ice. For these reasons the correlation between snow and ice thickness is only good for newly forming ice such as pancakes or nilas, as noted in the east early in the growth season. In general, the correlation between snow and ice thickness worsened in all sectors with increasing ice thickness. Ice core data presented in *Drinkwater and Haas* [1994] show that increases in ice thickness above

0.5 m may be due as much to rafting as to the slower process of thermodynamic growth (although this is likely not the case for multiyear ice). This factor, whereby snow would have less time to accumulate compared to on equal thickness ice grown thermodynamically, is noted elsewhere in Antarctica [*Allison and Worby*, 1994].

Cyclical variability of atmospheric conditions is also reflected in the complexity of observed snow properties. Periodic synoptic-scale fluctuations in air temperature, related to the passage of storms and the subsequent return to anticyclonic conditions, drive frequent reversals in snow vertical temperature gradient. These have a significant effect on snow structure, density, grain size, and thermal conductivity [*Sturm et al.*, 1996] by inducing cycling between high- and low-temperature gradient metamorphism, enhanced by the ready availability of moisture at the snow-ice interface which acts as an important vapour source. Such fluctuations increase in intensity with decreasing latitude. These observations are consistent with those of *Sturm et al.* [1996] in the Amundsen and Ross Seas in the winter of 1994 and *Jeffries et al.* [1994a] in the Bellingshausen Sea in 1993.

The overall mean snow density of 0.32 g cm^{-3} compares with that of 0.29 g cm^{-3} for the WWGS '89 experiment in September–October 1989 [*Eicken et al.*, 1994] but varied from 0.25 ± 0.06 g cm^{-3} in the eastern coastal sector to 0.37 ± 0.07 g cm^{-3} in the northwest. The greater textural assemblage of snow types present in the northwest may again be partly a function of relative lateness in the season but may also be due to the fact that the region contains perennial ice in an outflowing branch of the Weddell Gyre. The increasing prevalence of multiple icy layers is testament to the high degree of atmospheric variability experienced by the snow from initial deposition to eventual melt. Observations from the northwestern Weddell Sea indicate that melt-freeze cycles do not occur exclusively in spring and summer but that they are also an important feature of winter; both rain and near-zero air temperatures were encountered in the northwest in late July during WWGS '92. These findings are consistent with those in the Amundsen and Ross Seas in September–October 1994 of *Sturm et al.* [1996], who observed an increase in ice layering with decreasing latitude and proximity to the ice edge.

Although they form a small proportion of the overall snow volume, surface crusts are a widespread and significant feature. Forming quickly, they effectively cap and stabilize the underlying snow cover to negate further aeolian redistribution. When buried, they act as foci for ice layer formation. Were it not for the cyclical generation of such features, combined with rapid snow metamorphism, the magnitude and temporal and spatial variability of snow deposition into open leads would be considerably larger. As *Eicken et al.* [1994] point out, the component of drifting snow precipitated in leads has important implications for the freshwater (salinity) budget of ocean surface waters.

Widespread flooding was previously reported in this region for September–October [*Eicken et al.*, 1994]. The present study encountered less flooding overall (8% compared to 40%), with the majority of observations being in the central to northwestern Weddell Sea and largely associated with thicker ice with a thick snow cover. This apparent discrepancy may be due to the relative earliness of the present experiment and the fact that older ice floes, originating further south and having a potentially greater snow loading, had not yet drifted northward into the transect sampling locations elsewhere. Similar findings related to earliness in the season have been reported from East Antarctica [*Worby and Massom*, 1995]. It is thus difficult to draw conclusions about interannual variability from the current data set, which represents a series of snapshots. *Lytle and Ackley* [1996], presenting results from Ice Station Weddell, showed that the isostacy of a given floe constantly readjusts to freezing of slush from above and melt/freeze from below in response to changing conditions. As *Eicken et al.* [1995] point out, it is the evolution of ice freeboard that affects flooding and snow-ice formation. The permeability of the underlying ice is also a prerequisite for flooding where negative freeboards occur locally [*Eicken et al.*, 1994]. Ice permeability is a function of salinity and temperature; periodic increases in ice temperature in response to observed variations in air temperature may act to increase the permeability, but this remains to be validated. Alternatively, cracks formed during ice deformation may form paths along which seawater can migrate and flood onto the ice surface (V. Lytle, personal communication, 1996). Observations suggest that while snow loading is an important mechanism for inducing snow-ice formation, other processes related to ice deformation are also responsible for depressing the ice surface and causing flooding. Enhanced accumulation around ridges may compound the load and flooding. Thus distinctions should be made between regions of deformed and undeformed ice when assessing the impact of flooding and its contribution to the mass balance of the pack, as suggested by *Lange and Eicken* [1991].

In spite of the apparent discontinuity of flooding, the presence of a damp saline (>10‰) substrate at the snow base was a widely recorded phenomenon. It has important implications for remote sensing [*Hallikainen and Winebrenner*, 1992], snow-ice formation, and melt/freeze rates; snow salinities of 10‰ and 48‰ (the maximum snow salinity recorded) would raise the melting point/depress the freezing point of the snow to −0.57°C and −2.7°C, respectively. Moreover, it modifies snow dielectric properties, grain size distribution, melting point, density upon freezing, and the degree of bonding between ice and snow (and thus the centimeter-scale ice surface roughness). Observations suggest that even though newer ice forms have a positive freeboard, brine expelled upward during ice formation is available at their surface for vertical uptake into an accumulating snow cover by capillary suction (wicking). Salinity concentrations of >34‰ occur where high-salinity frost flowers are incorporated into the accumulating snow cover.

The effect of salinity on snow metamorphism, particularly depth hoar formation, may be significant but remains unresolved in this experiment. In order to address this question, we need more information about the distribution and nature of salinity in the snow mass; is the brine equally distributed within a given horizon, or is it contained in droplets, forming saline "nests" within an otherwise fresh snow?

An improved understanding of snow cover properties and thickness distribution on seasonal and regional scales is a prerequisite to improved retrievals of sea ice geophysical parameters from satellite microwave data (i.e., from the DMSP special sensor microwave/imager (SSM/I) and the ERS 1 and 2 SARs and scatterometer) and regional simulations in sea ice models. The present observations are limited by being snapshots in space and time but have highlighted large-scale snow variability. The improved resolution and monitoring of changes in the snow-ice cover and their relationship to ageing processes and possible regional and temporal differences in

precipitation patterns will require the setting up of ice camps similar to that described by *Gordon et al.* [1993]. Repeat visits are necessary to determine possible interannual variability.

Acknowledgments. The authors sincerely thank Captain Jonas and the crew of RV *Polarstern* and the helicopter crew on WWGS '92. We are very grateful to the voyage leader Peter Lemke, Marcus Thomas, the late Thomas Viehoff (all of the Alfred-Wegener Institut), and Petra Heil of the University of Kiel (now at the Antarctic CRC) for their vigorous participation/support in the experiment and to Joey Comiso of NASA Goddard Space Flight Center for his help and support of R. M. This paper benefited greatly from excellent comments by Vicky Lytle, Tony Worby, and Ian Allison of the Antarctic Cooperative Research Centre and from Jackie Richter-Menge of CRREL (Associate Editor of *JGR-Oceans*), Sam Colbeck (CRREL), Richard Armstrong (NSIDC/CIRES), and Eric Brun (Centre d'Etudes de la Neige) at the review stage. The work was carried out while R. M. was a U.S. National Research Council Resident Research Associate in the Oceans and Ice Branch (Code 971), NASA Goddard Space Flight Center. M. D. conducted this work at the Jet Propulsion Laboratory, California Institute of Technology, under contract to NASA. The authors are very grateful for the support of these organisations. This paper is dedicated to the memory of our friend and colleague, the late Al Lohanick, whose enthusiasm, professionalism, and kindness were central to the success of this experiment. This is Alfred-Wegener-Institut für Polar- und Meeresforschung contribution 1084.

References

Ackley, S. F., M. A. Lange, and P. Wadhams, Snow cover effects on Antarctic sea ice thickness, in *Sea Ice Properties and Processes, CRREL Monogr. 90-1*, edited by S. F. Ackley and W. F. Weeks, pp. 16–21, U.S. Army Corps of Eng., Hanover, N. H., 1990.

Ackley, S. F., A. J. Gow, V. I. Lytle, N. E. Yankielun, and M. N. Darling, Sea ice investigations on *Nathaniel B. Palmer*: Cruise 92-2, *Antarc. J. U. S.*, *27*, 87–88, 1992.

Allison, I., and A. P. Worby, Seasonal changes of sea-ice characteristics off East Antarctica, *Ann. Glaciol.*, *20*, 195–201, 1994.

Allison, I., R. E. Brandt, and S. G. Warren, East Antarctic sea ice: Albedo, thickness distribution and snow cover, *J. Geophys. Res.*, *98*(C7), 12,417–12,429, 1993.

Andreas, E. L., A theory for the scalar roughness and the scalar transfer coefficients over snow and sea ice, *Boundary Layer Meteorol.*, *38*, 159–184, 1987.

Andreas, E. L., M. A. Lange, S. F. Ackley, and P. Wadhams, Roughness of Weddell Sea ice and estimates of the air-ice drag coefficient, *J. Geophys. Res.*, *98*(C7), 12,439–12,452, 1993.

Banke, E. G., S. D. Smith, and R. J. Anderson, Drag coefficients at AIDJEX from sonic anemometer measurements, in *Sea Ice Processes and Models*, edited by R. S. Pritchard, pp. 430–442, Univ. of Wash. Press, Seattle, 1980.

Casarini, M. P., Winter Weddell Gyre Study, Polarstern (ANT VIII/2), 1989, special report, 171 pp., Scott Polar Res. Inst., Cambridge, England, 1990.

Casarini, M. P., and R. A. Massom, Winter Weddell Sea Project; sea ice observations, Leg 2: June–Sept. 1986, special report, 162 pp., Scott Polar Res. Inst., Cambridge, England, 1987.

Colbeck, S. C., An overview of seasonal snow metamorphism, *Rev. Geophys.*, *20*(1), 45–61, 1982.

Colbeck, S. C., Snow-crystal growth with varying surface temperatures and radiation penetration, *J. Glaciol.*, *35*, 23–29, 1989.

Colbeck, S. C., The layered character of snow covers, *Rev. Geophys.*, *29*(1), 81–96, 1991.

Colbeck, S., E. Akitaya, R. Armstrong, H. Gubler, J. Lafeuille, K. Lied, D. McClung, and E. Morris, *The International Classification for Seasonal Snow on the Ground*, 23 pp., Int. Glaciol. Soc., Cambridge, England, 1990.

Comiso, J. C., Sea ice effective microwave emissivities from satellite passive microwave and infrared observations, *J. Geophys. Res.*, *88*(C12), 7686–7704, 1983.

Drinkwater, M. R., LIMEX '87 ice surface characteristics: Implications for C-band SAR backscatter signatures, *IEEE Trans. Geosci. Remote Sens.*, *27*(5), 501–513, 1989.

Drinkwater, M. R., Applications of SAR measurements in ocean-ice-atmosphere interaction studies, in *Oceanographic Applications of Remote Sensing*, edited by M. Ikeda and F. W. Dobson, pp. 381–396, CRC Press, Boca Raton, Fla., 1995.

Drinkwater, M. R., and G. B. Crocker, Modelling changes in the dielectric and scattering properties of young snow-covered ice at GHz frequencies, *J. Glaciol.*, *34*, 274–282, 1988.

Drinkwater, M. R., and C. Haas, Snow, sea-ice, and radar observations during ANT X/4: Summary data report, *Ber. Fachber. Phys.*, *53*, 51 pp., Alfred-Wegener-Inst. für Polar- und Meeresforsch., Bremerhaven, Germany, 1994.

Drinkwater, M. R., R. Hosseinmostafa, and W. Dierking, Winter microwave radar scatterometer sea ice observations in the Weddell Sea, Antarctica, *Proceedings IGARSS '93*, vol. 2, pp. 446–448, Inst. of Electr. and Electr. Eng., Piscataway, N. J., 1993a.

Drinkwater, M. R., D. G. Long, and D. S. Early, Enhanced resolution scatterometer imaging of Southern Ocean sea ice, *ESA J.*, *17*, 307–322, 1993b.

Drinkwater, M. R., R. Hosseinmostafa, and P. Gogineni, C-band backscatter measurements of winter sea ice in the Weddell Sea, Antarctica, *Int. J. Remote Sens.*, *16*(17), 3365–3389, 1995.

Eicken, H., The role of sea ice in structuring Antarctic ecosystems, *Polar Biol.*, *12*, 3–13, 1992.

Eicken, H., M. A. Lange, H.-W. Hubberton, and P. Wadhams, Characteristics and distribution patterns of snow and meteoric ice in the Weddell Sea and their contribution to the mass balance of sea ice, *Ann. Geophys.*, *12*, 80–93, 1994.

Eicken, H., H. Fischer, and P. Lemke, Effects of the snow cover on Antarctic sea ice and potential modulation of its response to climate change, *Ann. Glaciol.*, *21*, 369–376, 1995.

Garrity, C., Characterization of snow on floating ice and case studies of brightness temperature changes during the onset of melt, in *Microwave Remote Sensing of Sea Ice, Geophys. Monogr. Ser.*, vol. 68, edited by F. Carsey, pp. 313–328, AGU, Washington, D. C., 1992.

Gloersen, P., W. J. Campbell, D. J. Cavalieri, J. C. Comiso, C. L. Parkinson, and H. J. Zwally, Arctic and Antarctic Sea Ice, 1978–1987: Satellite Passive-Microwave Observations and Analysis, *NASA Spec. Publ., SP-511*, 290 pp., 1992.

Gordon, A. L., and B. A. Huber, Southern Ocean winter mixed layer, *J. Geophys. Res.*, *95*(C7), 11,655–11,672, 1990.

Gordon, A. L., and Ice Station Weddell Group of Principal Investigators and Chief Scientists, Weddell Sea exploration from ice station, *Eos Trans. AGU*, *74*(11), 121, 124–126, 1993.

Haas, C., T. Viehoff, and H. Eicken, Sea-ice conditions during the Winter Weddell Gyre Study 1992, ANT X/4, with RV "Polarstern": Shipboard observations and AVHRR satellite imagery, *Ber. Fachber. Phys.*, *34*, 85 pp., Alfred-Wegener-Inst. für Polar- und Meeresforsch., Bremerhaven, Germany, 1992.

Hallikainen, M., and D. P. Winebrenner, The physical basis for sea ice remote sensing, in *Microwave Remote Sensing of Sea Ice, Geophys. Monogr. Ser.*, vol. 68, edited by F. Carsey, pp. 29–46, AGU, Washington D. C., 1992.

Hosseinmostafa, A. R., V. I. Lytle, K. C. Jezek, S. P. Gogineni, S. F. Ackley, and R. K. Moore, Comparison of radar backscatter from Antarctic and Arctic sea ice, *J. Electromagn. Waves Appl.*, *9*(3), 421–438, 1995.

Jeffries, M. O., K. Morris, A. P. Worby, and W. F. Weeks, Late winter characteristics of the seasonal snow cover on sea-ice floes in the Bellingshausen and Amundsen Seas, *Antarct. J. U.S.*, *29*, 9–10, 1994a.

Jeffries, M. O., A. L. Veazey, K. Morris, and H. R. Krouse, Depositional environment of the snow cover on West Antarctic pack-ice floes, *Ann. Glaciol.*, *20*, 33–38, 1994b.

Jordan, R., A one-dimensional temperature model for a snow cover; technical documentation for SNTHERM.89, *CRREL Spec. Rep. 91-16*, U.S. Army Corps of Eng., Hanover, N. H., 1991.

Lang, R. M., B. R. Leo, and R. L. Brown, Observations on the growth process and strength characteristics of surface hoar, paper presented at the International Snow Science Workshop, Mountain Rescue-Aspen, Aspen, Colo., 1984.

Lange, M., and H. Eicken, The sea ice thickness distribution in the northwestern Weddell Sea, *J. Geophys. Res.*, *96*(C3), 4821–4837, 1991.

Lange, M. A., S. F. Ackley, P. Wadhams, G. S. Dieckmann, and H. Eicken, Development of sea ice in the Weddell Sea, Antarctica, *Ann. Glaciol.*, *12*, 92–96, 1989.

Lange, M. A., P. Schlosser, S. F. Ackley, P. Wadhams, and G. S.

Dieckmann, ^{18}O concentrations in sea ice of the Weddell Sea, Antarctica, *J. Glaciol.*, *36*, 315–323, 1990.

Ledley, T. S., Snow on sea ice: Competing effects in shaping climate, *J. Geophys. Res.*, *96*(D9), 17,195–17,208, 1991.

Lemke, P. (Ed.), The expedition Antarktis X/4 of RV "Polarstern" in 1992, *Rep. Polar Res.*, *140*, 90 pp., Alfred-Wegener-Inst. für Polar- und Meeresforsch., Bremerhaven, Germany, 1994.

Livingstone, C., K. Singh, and A. Gray, Seasonal and regional variations of active/passive microwave signatures of sea ice, *IEEE Trans. Geosci. Remote Sens.*, *GE-25*(2), 159–173, 1987.

Lohanick, A. W., Some observations of established snow cover on saline ice and their relevance to microwave remote sensing, in *Sea Ice Properties and Processes*, edited by S. F. Ackley and W. F. Weeks, *CRREL Monogr. 90-1*, pp. 61–67, U.S. Army Corps of Eng., Hanover, N. H., 1990.

Lohanick, A. W., Microwave brightness temperatures of laboratory-grown undeformed first-year ice with an evolving snow cover, *J. Geophys. Res.*, *98*(C3), 4667–4674, 1993.

Lytle, V. I., and S. F. Ackley, Snow properties and surface elevation profiles in the Western Weddell Sea, (NBP92-2), *Antarct. J. U.S.*, *27*, 93–94, 1992.

Lytle, V. I., and S. F. Ackley, Heat flux through sea ice in the western Weddell Sea: Convective and conductive transfer processes, *J. Geophys. Res.*, *101*(C4), 8853–8868, 1996.

Massom, R., Observing the advection of sea ice in the Weddell Sea using buoy and satellite passive microwave data, *J. Geophys. Res.*, *97*(C10), 15,559–15,572, 1992.

Mätzler, C., H. Äbnischer, and E. Schanda, Microwave dielectric properties of surface snow, *IEEE J. Oceanic Eng.*, *OE-9*(5), 333–338, 1984a.

Mätzler, C., R. Ramseier, and E. Svendsen, Polarization effects in sea-ice signatures, *IEEE J. Oceanic Eng.*, *OE-9*(5), 366–371, 1984b.

Maykut, G., The surface heat and mass balance, in *Geophysics of Sea Ice*, *NATO ASI Ser., Ser. B*, vol. 146, edited by N. Untersteiner, pp. 395–463, Plenum, New York, 1986.

Meese, D. A., J. W. Govoni, and S. F. Ackley, Snow and sea-ice thicknesses: Winter Weddell Gyre Study, 1989, *Antarct. J. U.S. 1990 Rev.*, *25*, 116–117, 1990.

Moore, M. B., Temperature gradient weakening of snowpacks near rain crusts or melt-freeze layers, paper presented at International Snow Science Workshop, Montana State Univ., Bozeman, Oct. 21–23, 1982.

Owens, W. B., and P. Lemke, Sensitivity studies with a sea ice-mixed layer-pycnocline model in the Weddell Sea, *J. Geophys. Res.*, *95*(C6), 9527–9538, 1990.

Perovich, D. K., and J. A. Richter-Menge, Surface characteristics of sea ice, *J. Geophys. Res.*, *99*(C8), 16,341–16,350, 1994.

Sturm, M., The role of thermal convection in heat and mass transport in the sub-Arctic snow cover, *CRREL Rep. 91-09*, 84 pp., U.S. Army Corps of Eng., Hanover, N. H., 1991.

Sturm, M., K. Morris, and R. Massom, A description of the snow cover on the winter sea ice of the Amundsen and Ross Seas, *Antarct. J. U.S.*, *30*, 1–4, 1996.

Sturm, M., K. Morris, and R. Massom, The character and distribution of the winter snow cover on the sea ice of the Bellingshausen, Amundsen and Ross Seas, Antarctica, 1994–1995, in *Antarctic Sea Ice: Physical Properties and Processes*, *Antarct. Res. Ser.*, edited by M. O. Jeffries, AGU, Washington, D. C., in press, 1997.

Sullivan, C. W., A. C. Palmisano, S. T. Kottmeier, S. McGrath Grossi, and R. Moe, The influence of light on growth and development of the sea-ice microbial community of McMurdo Sound, in *Antarctic Nutrient Cycles and Food Webs*, edited by W. R. Siegfried, P. R. Condy, and R. M. Laws, pp. 84–88, Springer-Verlag, New York, 1985.

Wadhams, P., M. A. Lange, and S. F. Ackley, The ice thickness distribution across the Atlantic sector of the Antarctic Ocean in midwinter, *J. Geophys. Res.*, *92*(C13), 14,535–14,552, 1987.

Worby, A. P., and R. A. Massom, The structure and properties of sea ice and snow cover in East Antarctic pack ice, *Antarctic CRC Res. Rep. 7*, 191 pp., Antarct. Coop. Res. Cent., Hobart, Tasmania, Australia, 1995.

Worby, A. P., W. F. Weeks, M. O. Jeffries, K. Morris, and R. Jaña, Late winter sea ice and snow thickness distribution in the Bellingshausen and Amundsen Seas, *Antarct. J. U.S.*, *29*, 13–15, 1994.

Yen, Y. C., Review of thermal properties of snow, ice and sea water, *CRREL Rep. 8-10*, U.S. Army Corps of Eng., Hanover, N. H., 1981.

M. R. Drinkwater, NASA Jet Propulsion Laboratory, California Institute of Technology, 4800 Oak Grove Drive, Pasadena, CA 91109.

C. Haas, Alfred Wegener Institute für Polar- und Meeresforschung, Columbusstrasse, D 27570 Bremerhaven, Germany.

R. A. Massom, Antarctic Cooperative Research Centre, University of Tasmania, GPO Box 252-80, Hobart, Tasmania 7001, Australia. (e-mail: r.massom@antcrc.utas.edu.au)

(Received March 11, 1996; revised June 25, 1996; accepted July 1, 1996.)